applied sciences

MDPI

Article

Proof of Concept of Reconfigurable Solvent Vapor Sensor Tag with Wireless Power Transfer for IoT Applications

Houda Ayadi [1], Jan Machac [2], Milan Svanda [2,*], Noureddine Boulejfen [3] and Lassaad Latrach [1]

[1] Department of Physics, Microwave Electronics Research Laboratory, Faculty of Sciences of Tunis, University of Tunis El Manar, Tunis 2092, Tunisia
[2] Department of Electromagnetic Field, Faculty of Electrical Engineering, Czech Technical University in Prague, Technicka 2, 16627 Prague, Czech Republic
[3] Military Research Center, Taieb Mhiri City, Tunis 2045, Tunisia
* Correspondence: svanda.milan@fel.cvut.cz

Abstract: In this paper, a concept of a reconfigurable chipless radio frequency identification (RFID) sensor tag for detecting solvent vapors/gas in IoT applications was presented. The concept was based on the authors' previously published rectangular loop structure equipped with a U-folded dipole loaded with a glide-symmetrical interdigital capacitor coated with a thin layer of tetrasulfonated copper phthalocyanine deposited as a sensing layer to improve the sensing capability in the presence of acetone vapor. In order to further maximize the sensitivity of the designed structure to the desired solvent, a circuit for a central frequency adjustment using a radio frequency varactor diode biased with a wireless power transfer (WPT) was designed. By varying the DC bias of the diode, a continuous tunable range of approximately 200 MHz was achieved. The proposed reconfigurable wireless sensor tag was manufactured and the frequency shift was verified by measurement. The proposed external frequency control can be applied to a wide class of electrical resonators.

Keywords: chipless RFID; gas sensor; glide symmetry; Internet of Things (IoT); reconfigurability; U-folded dipole; varactor diode; wireless power transfer (WPT)

check for updates

Citation: Ayadi, H.; Machac, J.; Svanda, M.; Boulejfen, N.; Latrach, L. Proof of Concept of Reconfigurable Solvent Vapor Sensor Tag with Wireless Power Transfer for IoT Applications. *Appl. Sci.* **2022**, *12*, 10266. https://doi.org/10.3390/app122010266

Academic Editors: Ryan Gibson and Hadi Larijani

Received: 15 September 2022
Accepted: 8 October 2022
Published: 12 October 2022

Publisher's Note: MDPI stays neutral with regard to jurisdictional claims in published maps and institutional affiliations.

Copyright: © 2022 by the authors. Licensee MDPI, Basel, Switzerland. This article is an open access article distributed under the terms and conditions of the Creative Commons Attribution (CC BY) license (https://creativecommons.org/licenses/by/4.0/).

1. Introduction

Radio frequency identification (RFID) is a modern technology used to wirelessly transmit and receive data. It is widely employed in a variety of Internet of Things (IoT) applications such as automatic identification, tracking, access control, security surveillance, supply chain, healthcare, and sensing applications [1–3]. A combination of RFID tags and sensing components can finally provide identification and sensing functions with a wireless and contactless data transmission. Passive RFID sensors, the latest technology for wireless monitoring, take advantage of new and interesting solutions because the sensors are simple structures that are easy to integrate and cheap to produce.

Nevertheless, their silicon-free counterparts used for chipless sensing have also attracted particular attention because these sensors can be completely printed, which has the advantage of ultra-low manufacturing costs, thereby promoting the development of new IoT applications [4,5].

The chipless sensor is essentially composed of two elements: the radiator (scatterer) and the transducer, both of which are related to the sensitivity and readability of the sensor. Because the electrical permittivity of the sensitive layer or part of the sensor is sensitive to the environmental parameter being monitored, the information can be processed by monitoring the resonant frequency shift from the backscattered electromagnetic response of the sensor [6].

Due to the limited sensor life, power, and cost constraints of traditional wired and battery-powered sensors [7], realizing sensors based on wireless power transfer (WPT) has been a challenge. It can present a promising solution that has the potential to revolutionize the future world of rich IoT sensing. The WPT represents an effective method of delivering power wirelessly from a source to an appliance [8–10]. Thanks to the wide coverage and easy mobility of RFID readers, the measurement of “things” marked by RFID sensors is no longer limited to specific locations. Therefore, the information-reception process of the RFID sensors becomes far more flexible and convenient, and its applications are often extended to a wider range of fields [11].

Recently, the need for sensors to monitor environmental parameters in modern homes, vehicles, and industries has attracted a lot of interest. In the literature, several designs have been proposed for the sensing of temperature and humidity [12,13], gas concentration [14–16], and movement [17]. The availability of high-performing, reliable, and low-cost sensors is essential to facilitate the development of these applications (detection of gas, temperature, etc.) on a large scale and in a safe manner.

This paper focuses on passive gas sensors. Previous research has already dealt with the use of radio frequency (RF) technologies for the implementation of innovative gas sensors. In [18], gas detection was realized using microwave transmission lines. In this case, the response of the dielectric material under the application of a microwave signal and in the presence of gas was used as a microwave transducer. Other microwave structures have also been utilized in gas detection. In [19], the dielectric response of carbon nanotubes was used in a microwave resonator to indicate the presence of gases and determine their concentration. The dielectric response affects the spectrum of the device, which can be tracked in order to identify the type and concentration of gases to be detected. Ashraf et al. proposed in [20] an environmental gas sensor using a microwave resonator based on substrate-integrated waveguide; the sensor function was implemented by functionalizing a specific region inside the resonator. Other approaches such as the use of a waveguide and printed LC (electric circuit consisting of an inductor L and a capacitor C) resonators and dielectric resonator-based filters have also been employed to design gas sensors, as described in [21].

Several sensors for acetone vapor sensing operating in the microwave frequency band, which is directly related to the solution presented in this paper, have been published in the literature [22–25]. The main drawback of the solutions published in [22,24,25] was that they were not contactless detection, but used direct measurement of the microwave transmission line to detect the response. Although the solution in [23] was contactless, the overall RCS response level was quite low (-30 dBsm) and consequently, the structure of the reader antenna had to be placed in close proximity (within about 15 mm).

In some situations, chipless RFID gas sensors may be subject to multiple factors that may affect their behavior or require a modification of their characteristics or a variation in frequency to adapt to their environment and achieve nominal results. In such situations, the effective solution is to incorporate the concept of agility in the sensing applications. Agility can be achieved either by the physical sensor itself when it is used as a control unit to sense variations in the surrounding environment [26,27] or by RF elements including PIN diodes [28], microelectromechanical system (MEMS) switches [29], and varactor diodes [30].

The present paper introduces a proof of concept of frequency adjustment of a chipless radio frequency identification (RFID) sensor tag for detecting solvent vapors/gas using a wireless power transfer (WPT). The concept was based on the authors’ previously published rectangular loop structure equipped with a U-folded dipole loaded with a glide-symmetrical interdigital capacitor coated with a thin layer of tetrasulfonated copper phthalocyanine deposited as a sensing layer to improve the sensing capability in the presence of acetone vapor. In order to further maximize the sensitivity of the designed structure to the desired solvent, a circuit for a central frequency adjustment using a radio frequency varactor diode biased with a wireless power transfer (WPT) was designed. In principle, different gases and sensitive layers can be differently sensitive at different frequencies. To find the appropriate frequency, the resonant dip detuning option can then be used. The aim of this paper was to present a custom transponder geometry that potentially offered this possibility.

The paper is organized as follows. Section 2 is devoted to a detailed presentation of the static version of the proposed sensor and a description of a reconfigurability solution based on the WPT system. Section 3 covers an experimental validation of the sensor and describes the fabricated prototype, measurement setups, and measurement results along with their interpretation. Finally, Section 4 is reserved for conclusions.

2. Reconfigurable RFID Sensor for Detecting Solvent Vapors/Gas

2.1. Operating Principles of the Chipless RFID Sensor

Generally, in a chipless sensor system based on electromagnetic transduction, two main modules can be identified. A reader sends an interrogation signal and a sensor tag responds with a backscattered signal in a spectrum containing the sensed data [31]. The chipless RFID sensor reader initiates the operation by sending an interrogation signal to the chipless RFID sensor tag. The chipless RFID tag, which serves as a sensing unit, then immediately reflects the impact signal, which generates a backscattered signal containing the sensed information. The scattered signal is then received and analyzed by the reader. The electromagnetic transduction employs an RF transducer to convert the physical parameters that are being sensed into RF parameters that can be easily detected by remote systems. When an RF sensor is deployed in an environment to detect the presence of or changes in a specific natural phenomenon, its RF parameters such as the resonant frequency or RF impedance will change accordingly. A change in RF parameters subsequently affects the sensor response such as its radar cross section (RCS). This in turn affects the spectral signature of the scattered signal, which carries information about the physical parameters that are being sensed such as temperature, the presence of gas and its type, moisture, etc. The modified scattered RF signal is then received by the RFID reader and the transferred information is measured and analyzed.

2.2. Sensor

There have been many efforts in recent years to develop LC sensors for different applications, including gas detection. The present research focused on LC-type passive sensors because they are simple structures with favorable electrical characteristics.

The proposed sensor was based on a printed LC resonator with a dielectric layer sensitive to gas. The resonator was realized by a U-folded dipole (UD) terminated by a glide-symmetrical interdigital capacitor (IC-UD) [31]. The resonator was designed on the Kapton substrate Dupont Pyralux AP 8515R with a dielectric constant of 3, a thickness of 25 µm, and a loss tangent of 0.002. The standard commercially applied PCB etching technology was used to fabricate the sensor test sample. The copper metallic layer's thickness was 18 µm. To sensitize the resonator to the presence of acetone vapors, a sensitive phthalocyanine layer was applied and placed on the top of the UD resonator area for experimental validation and around the resonator for simulation. Finally, the resonator was placed inside a rectangular metallic loop in order to raise the overall RCS level of the tag. The advantages of the IC-UD such as its small electrical size, high sensitivity, and high quality factor were demonstrated in [14], in which the effect of the number of fingers of the IC and the position of the IC-UD inside the loop also were investigated. The resulting structure and the dimensions of the sensor tag are presented in Figure 1 and Table 1, respectively. The figure shows that the metallic loop was cut by an interdigital capacitor, the purpose of which is discussed in the next section.

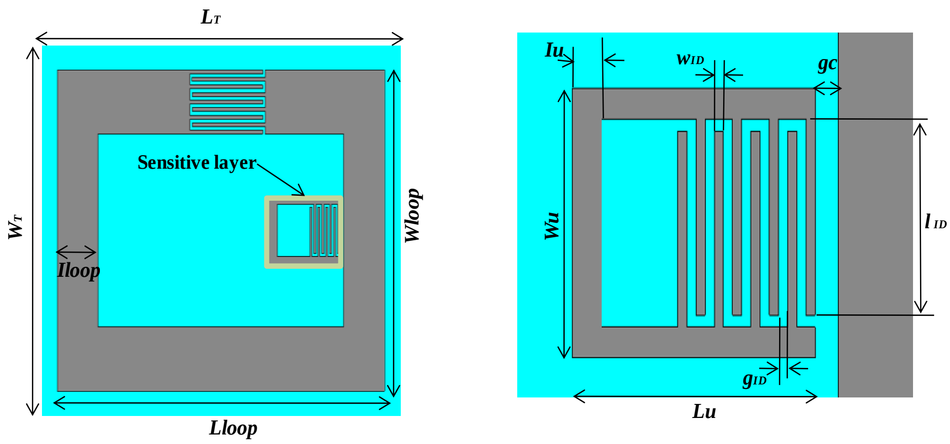

(**a**) (**b**)

Figure 1. Layout of the proposed RFID chipless sensor: (**a**) IC-UD coupled inside the metallic loop; (**b**) resonant element. Blue—dielectric kapton substrate; grey—copper layer.

Table 1. Dimensions of the sensor tag.

TAG (Dimensions in mm)					
L_T	W_T	L_{loop}	W_{loop}	I_{loop}	L_u
45	30	40	25	5	7.3
W_u	I_u	l_{ID}	w_{ID}	g_{ID}	g_c
4.4	0.5	3.2	0.2	0.2	0.5

The expression of the interdigital capacitance, as given in [32], is:

$$C = (\varepsilon_r + 1) l_{ID} [(N-3)A_1 + A_2] \text{ (pF)}, \quad (1)$$

where ε_r is the relative dielectric constant of the substrate, l_{ID} is the length of the interdigital capacitor finger, and N is the number of fingers. Next, A_1 and A_2 are the interior and exterior capacitances per unit length of the fingers, respectively. They can be approximately expressed as:

$$A_1 = 4.409 tanh\left[0.55\left(\frac{h}{w_{ID}}\right)^{0.45}\right] \times 10^{-6}\left(\frac{\text{pF}}{\mu\text{m}}\right), \quad (2)$$

$$A_2 = 9.92 tanh\left[0.52\left(\frac{h}{w_{ID}}\right)^{0.5}\right] \times 10^{-6}\left(\frac{\text{pF}}{\mu\text{m}}\right), \quad (3)$$

where h is the height of the substrate material and w_{ID} is the width of the fingers.

Figure 2 presents the RCS of the passive sensor tag when it was exposed to a plane wave. Two simulations; i.e., with and without the sensitive layer, were performed in computer simulation technology (CST) software. The IC-UD coupled to the loop provided a relatively high RCS level (−30 dBsm) at 3.2 GHz. This helped to detect the tag response at the desired distance range. A sensitive layer with a thickness of 100 µm and a relative dielectric constant of 3 was applied and simulated—the thickness of the sensitive layer for simulation purposes was chosen to be much higher than its real value. In fact, a very thin layer requires a high mesh resolution, which drastically increases the computation time. The simulation result shown in Figure 2 revealed that a small frequency shift ∆f (from 3.2 to 2.75 GHz) was obtained due to the presence of the sensitive layer. The effect of its thickness on the frequency shift will be experimentally verified in Section 3. In the experiments, the real sensitive layer's thickness was set to 6 and 12 µm.

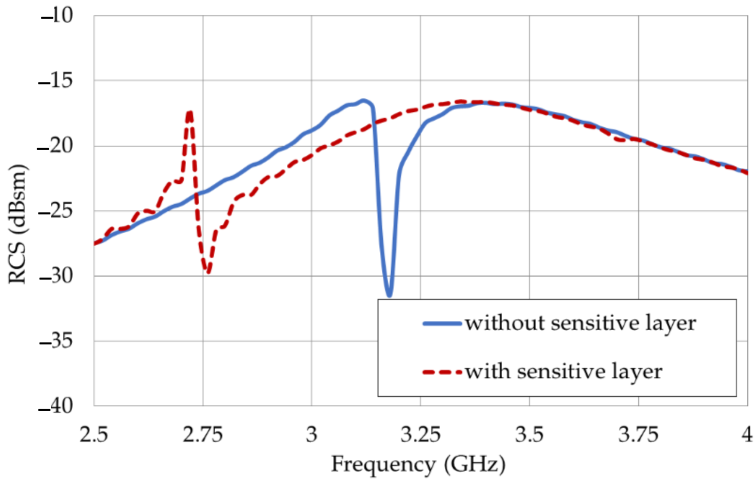

Figure 2. Simulated RCS of the chipless RFID tag with and without the sensitive layer.

The dielectric surrounding the UD resonator area had a minor influence on the frequency shift Δf. The resonant frequency of this structure also can be shifted using other techniques such as reconfigurability (agility), which enables the structure to vary its operating frequency.

2.3. Reconfigurable Resonant Frequency of the Sensor

Reconfigurable resonators offer the capability to change the resonator characteristics to adapt to dynamic wireless communication systems. The most significant characteristic is the resonant frequency, which is controlled by changing the capacitance of the resonator. Accordingly, different active RF elements such as PIN diodes [28], MEMS [29], and varactor diodes [30] can be used to change the capacitance of the resonator. In this paper, a varactor diode was selected because it could provide a continuous tuning of the resonant frequency of the sensor tag. Reconfigurability was used in order to obtain the optimal resonant frequency in which the sensor showed a maximum sensitivity to the environment. The varactor was placed into the resonant element and reverse biased through the WPT, which made the structure simple, since these types of feeding do not require wire connections. The resonant frequency of the resonator could be controlled by varying the reverse-bias voltage V_r, which was related to the variation in the diode capacitance. Figure 3 depicts the reconfigurable RCS of the chipless tag coupled to the loop and loaded with a Skyworks varactor diode (SMV1213) [33].

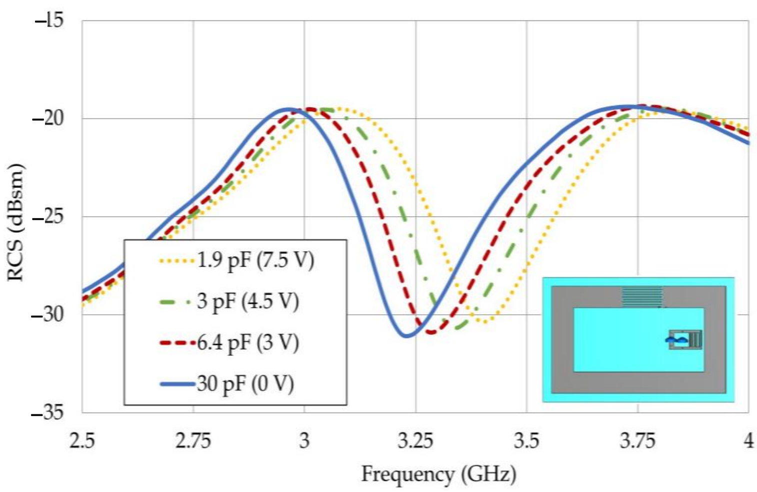

Figure 3. Simulated RCS for different values of varactor capacitances *C*.

For different values of C = [1.9, 3, 6.4, 30] pF that corresponded to V_r = [7.5, 4.5, 3, 0] V, respectively, the frequency was tuned from 3.2 to 3.4 GHz, which offered a tuning range of 200 MHz, which corresponded to more than 5% when compared to the reference resonant frequency. The voltage V_r that controlled the capacitance of the varactor was obtained by rectifying the signal collected by the receiving loop from the received EM wave. The sensor was treated here in a simplified version without the active layer merely as a proof of concept.

2.4. Varactor Diode Reverse Biasing

The process of RF energy transfer involves converting RF energy into DC energy for direct use to supply a low-power device [34]. The key element of the RF power transfer system is the rectifying antenna, also called a rectenna. It consists of a receiving antenna and an RF-to-DC rectifier. The performance of the rectenna is defined by the value of its output voltage and its RF-to-DC conversion efficiency. A variety of topologies can be used to convert RF power to DC power, such as a single diode in series or shunt, a voltage doubler circuit [35], or a bridge circuit [36]. For equivalent RF input power, the advantage of the voltage doubler circuit is that it can achieve a higher output voltage than a single diode configuration.

In the present paper, the aim was to rectify the signal obtained from the received wave of a frequency much lower than the sensor resonant frequency range and convert it into useful DC voltage to control the capacitance of the varactor. Accordingly, the suggested rectifier circuit presented in Figure 4 was a voltage doubler configuration using shunt-mounted (packaged SOT143) BAS3007A-RPP Schottky diodes [37]. The rectifier received the energy that came from the receiving antenna and was filtered by the capacitance C_1, then it converted the energy to DC voltage in order to power the varactor. Another capacitance, C_2, was placed across the output of the rectifier in parallel with the varactor diode and was used to smooth the output of the rectifier into a pure DC output signal. Coming out of C_2, the signal passed through the Zener diode D_Z, which was used as a voltage regulator; i.e., to limit the voltage reaching the varactor and protect it from damage. The signal then passed through a resistor in order to prevent the high-frequency signal of 3.2 GHz, at which the resonator worked, from leakage into the rectifying circuit; finally, the signal arrived at the D_V varactor diode to power it.

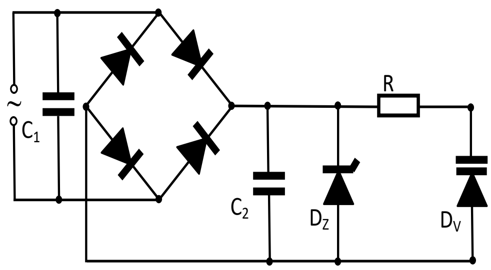

Figure 4. Rectifying circuit.

The above-described circuit was printed on the backside of the sensor tag (see Figure 5). The rectangular conducting loop, originally present to set up the appropriate level of the sensor RCS, was used as an antenna. This antenna received the low-frequency controlling signal of 7.2 MHz, which was then rectified and fed to the varactor to control its capacitance. The loop was cut by an interdigital capacitor to prevent DC short circuits. To incorporate the rectifying circuit, it was necessary to modify the geometry using both sides of the extremely thin substrate and appropriate placement of the conductive paths so that the high- and low-frequency parts did not negatively interfere with each other. Part of the modification also included the design of the capacitive loop and the U-dipole arm breaking for DC decoupling, again with a view toward avoiding negative interference (see Figure 5).

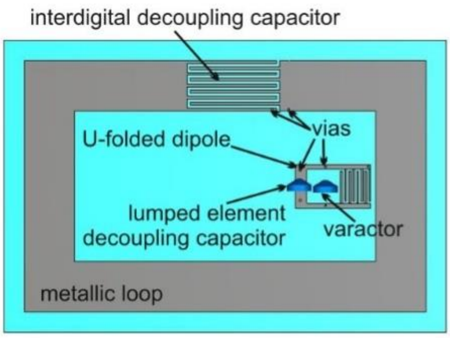

(**a**)

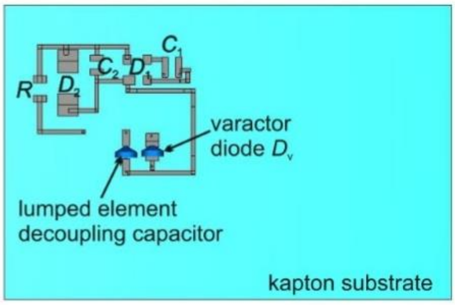

(**b**)

Figure 5. Layout of the proposed RFID chipless sensor tag: (**a**) top layer with U-folded dipole and metallic loop; (**b**) bottom layer with rectifying circuit. Blue—dielectric kapton substrate; grey—copper layer.

3. Results

3.1. Fixed Sensor Behavior

Following the design phase, the passive RFID sensor was manufactured on a 25 µm thick Kapton Dupont Pyralux AP 8515R substrate and a phthalocyanine active layer for sensing acetone vapors/gas was applied. To assess the performance of the proposed sensor in a more realistic scenario, experimental tests were performed in which tetrasulfonated copper phthalocyanine [14,38]—copper (II) phthalocyanine-3,4′,4′′,4′′′-tetrasulfonic acid tetrasodium salt, abbreviated as CuPcTS—was used as an active layer. This type of metallophthalocyanine was modified to improve its solubility and sensing response compared to the basic one, which suffered from a very low solubility in polar and non-polar solvents. The sensing response of basic metallophthalocyanines is based on the change in impedance in the presence of the detected gaseous analyte. A solution of the respective phthalocyanine in distilled water was prepared with a concentration of 1.45 mmol/l. Two thickness values of the sensitive layer, 0.6 µm and 1.2 µm, were used. The sensitive layer was applied on the surface of the IC-UD by pipetting and subsequent drying. The sensor tag sensitivity was verified by measurement inside a waveguide line with the Agilent E8364A vector network analyzer. The tag was inserted into an R32 waveguide chamber. This "test gas part" was separated from the adjacent parts of the measurement line by Tedlar membranes to hermetically isolate the solvent vapors, as illustrated in Figure 6. The acetone vapor with the specified concentration of 10,000 ppm in the synthetic air was introduced into the "test gas part" through a suction pump that drew it from the Tedlar bag.

Table 2 gives an overview of the measured scattering response of the IC-UD coupled to the loop and treated with the CuPcTS sensitive layer as measured by the reflection coefficient of the waveguide line both with and without the 10,000 ppm acetone vapor. In the presence of the acetone vapor, there were noticeable frequency shifts of 9 and 12 MHz caused by the sensitive phthalocyanine layer of 0.6 and 1.2 µm in thickness, respectively. The purpose of this comparison was only to verify the function and concept of resonant detuning using a varactor diode. Further optimization of the sensor and full calibration under different conditions may be the subject of future work.

Table 2. Measured frequency shifts depending on the sensitive phthalocyanine layer's parameters.

Phthalocyanine Layer Thickness (µm)	Frequency (GHz)	Δf (GHz)	Δf (%)
0.6 µm without acetone vapor	3.276	0.009	0.3
0.6 µm with acetone vapor	3.285		
1.2 µm without acetone vapor	3.264	0.012	0.4
1.2 µm with acetone vapor	3.276		

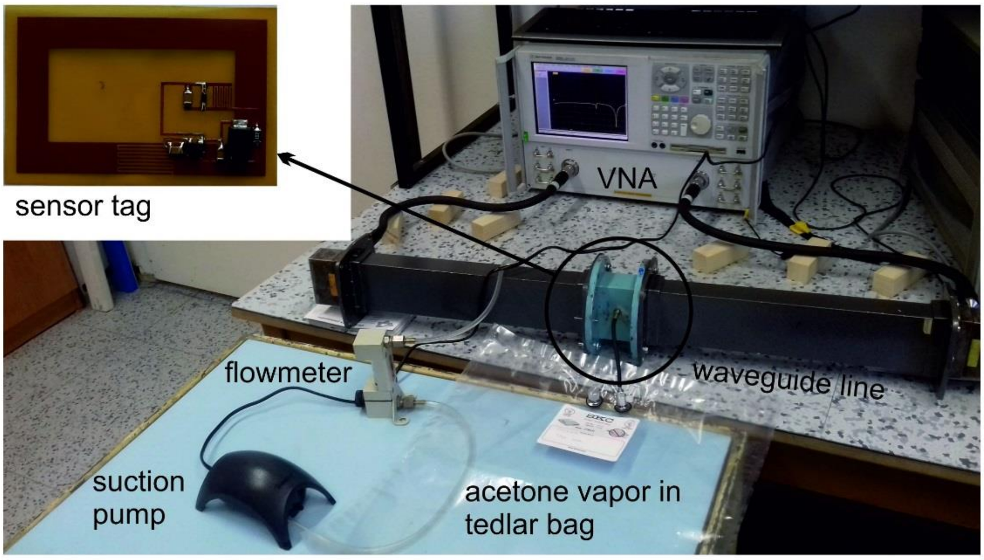

Figure 6. Photograph of the waveguide chamber measurement setup.

3.2. Tunable Sensor

As mentioned in Section 2, the reconfigurability of the RFID sensor was obtained by changing the DC voltage of the varactor diode that was fed by a WPT. Regarding the powering part, a wire loop operating at a frequency of 7.2 MHz—chosen to ensure acceptable dimensions of the loop—was used as a transmitting element for the WPT to the rectangular loop, which was used as a receiving element for the WPT on the part of the tag. The 7.2 MHz operating frequency also was chosen based on measuring the voltage needed to supply the capacitance of the varactor diode and the corresponding frequency, as shown in Figure 7. A maximum voltage of 3.8 V was achieved at a frequency of 7.2 MHz for $P_g = -20$ dBm (generator output) and $P_A = +31$ dBm (amplifier output).

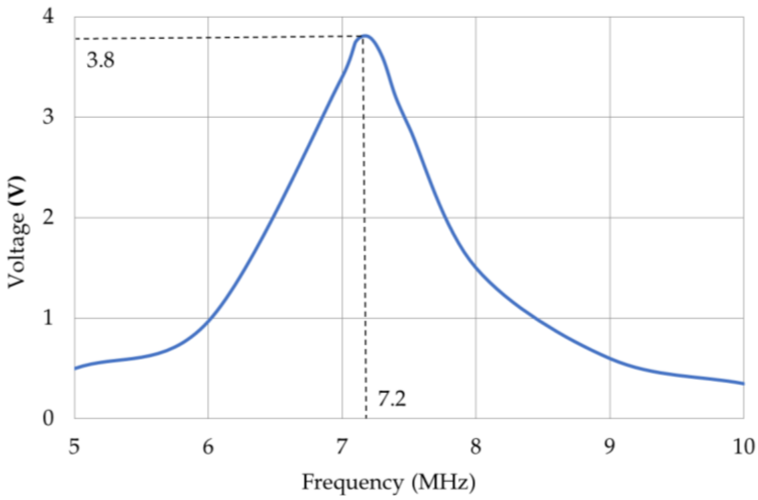

Figure 7. Measured rectified DC voltage and the corresponding frequency.

Figure 8 shows the measurement setup of the DC voltage at terminals of the varactor diode. An RF generator (SG 2000) in cascade with a power amplifier (BSA 0101-25/30D), a wire loop, a Voltcraft multimeter (M-4660A), and the sensor tag were used for the measurement. The components used for the measurements are listed in Table 3. The wire loop transmitted a WPT signal to the sensor tag to irradiate it. Then, the rectifier on the back side of the tag converted the energy captured by the rectangular tag loop serving as the receiving element into a DC voltage to bias the varactor diode. Finally, the voltage produced at the terminals of the diode was measured using the Voltcraft multimeter. The reactance of the transmitting loop was compensated by a capacitor value of C = 10 nF to form a parallel resonant circuit at an operating frequency of 7.2 MHz, which is a free industrial and medical frequency band. The resonant circuit ensured a purely resistive input impedance, as shown by the power amplifier.

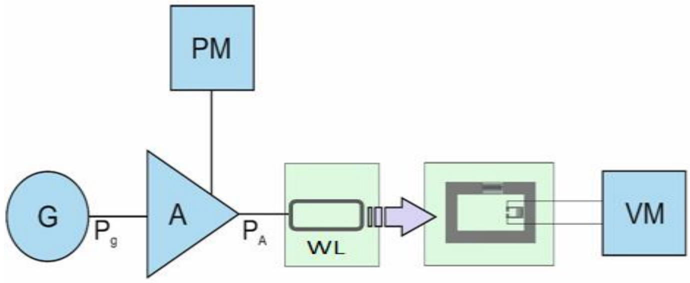

Figure 8. Setup for measuring the DC voltage of the varactor.

Table 3. The components used in the configuration of the DC voltage measurement.

G	Generator: Elsy SG 2000 (100 kHz–1 GHz)
A	Power amplifier: BONN Elektronik BSA 0101-25/30D (9 kHz–1 GHz, +46 dB)
PM	Power meter: Keysight (Hewlett-Packard) 437B + power sensor
WL	Wire loop
VM	Multimeter: Voltcraft M-4660A

Figure 9 presents the final prototype of the sensor tag coupled to the rectifying circuit. In this part, the maximum transmitted power (P_A) that could activate the varactor diode was measured. Based on the datasheet of the varactor, the V_r should be in the range of 0 to 8 V, providing a capacitance in the range of 1.9 to 30 pF.

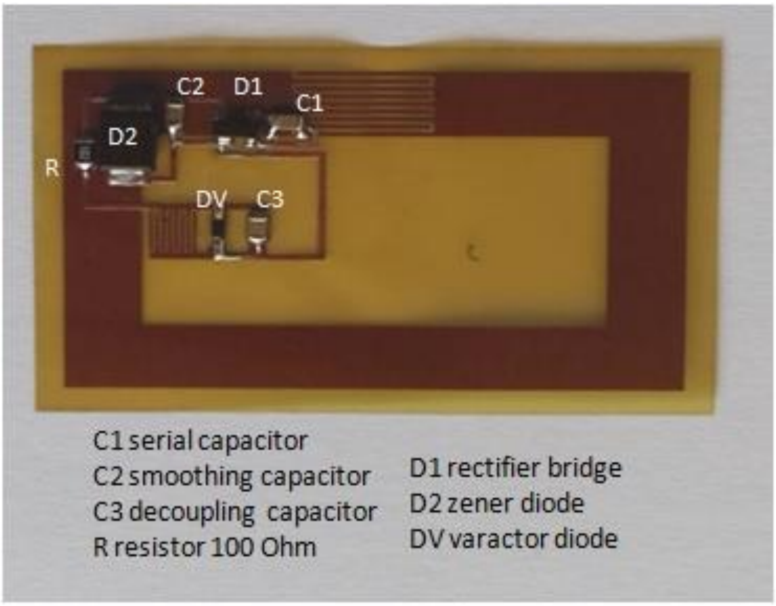

Figure 9. Prototype of the sensor tag coupled to the rectifying circuit.

Following from Table 4, the voltage needed for the diode to operate was achieved by adjusting the input energy of the generator. The maximum power needed here was 41 dBm, corresponding to about 12 W, which would later be rectified to a DC voltage to obtain 7.5 V, which was slightly below the limiting Zener voltage [39].

Table 4. Measured input power and the corresponding rectifier voltage.

#	P_g (dBm)	P_A (dBm)	V_r (V)
1	−40	10.9	0.35
2	−35	15.8	0.65
3	−30	20.9	1.40
4	−25	26.0	2.60
5	−20	31.0	3.80
6	−15	36.0	7.30
7	−10	41.0	7.50
8	−5	45.1	7.60
9	0	47.1	7.70

As previously mentioned, the power needed to irradiate the sensor tag was transmitted by the wire loop antenna and received by the rectangular loop on the side of the tag. The rectifier located on the back side of the structure converted the energy collected by the rectangular loop into a DC voltage (V_r) to bias the varactor diode. By changing the input energy, the DC voltage of the diode changed, which in turn caused a change in frequency, effectively changing the P_A needed to tune the resonant frequency of the sensor tag. The WPT system controlled the DC bias of the varactor diode. The polarization of the varactor diode in the reverse direction was defined by the controlling circuit; i.e., by the connection of rectifying diodes. The effect of the presence of gas on the stability of the control voltage V_r on the varactor could be considered negligible. The gas being detected had a very low concentration (10,000 ppm), which only negligibly altered the effective permittivity of the surrounding environment and therefore could not adversely affect the WPT system. Actual gas detection was only possible due to the sensitive interdigital structure of the resonator, which was only minimally coupled to the power supply (nf separation in the loop).

Then, a horn antenna was added to the wireless system, as illustrated in Figure 10. The horn antenna listed in Table 5 operates as a dual transmitting/receiving antenna for the RFID reader and was used to communicate with the sensor tag. Figure 11 presents the measurement setup in an anechoic chamber.

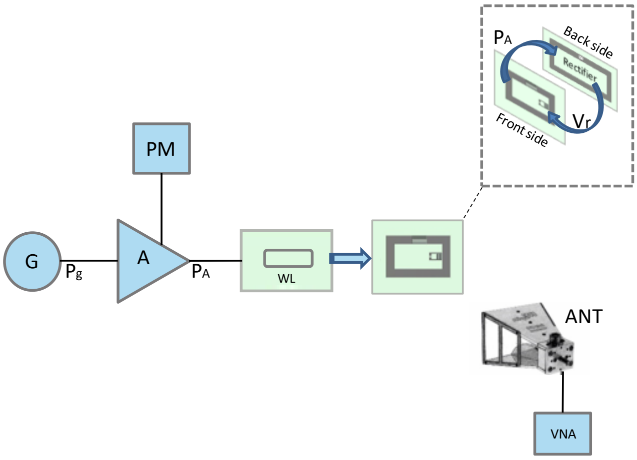

Figure 10. Schematic diagram of the entire system.

Table 5. The components used for communication with the sensor tag.

VNA	Vector network analyzer: Rohde & Schwarz ZVA40 (10 MHz–40 GHz)
ANT	Double-ridged horn antenna: DRH20 (1.7–20 GHz)

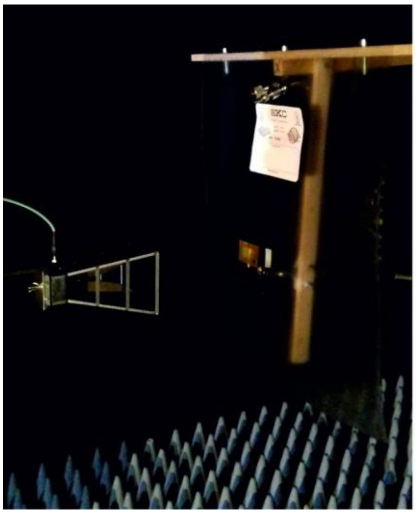

(a)

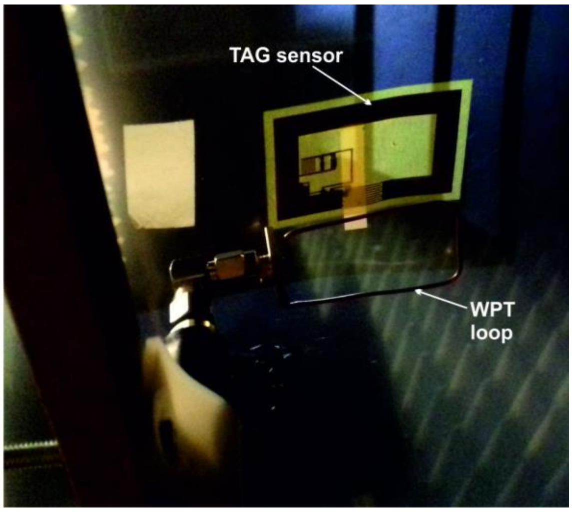

(b)

Figure 11. Measurement setup in an anechoic chamber: (**a**) front view of RFID tag and measuring antenna; (**b**) back view of RFID tag and WPT loop.

Figure 12 depicts the measured RCS response of the tag in an anechoic chamber in which a monostatic measurement with the Rohde & Schwarz ZVA40 network analyzer was performed. The operation of the tag was based on an evaluation of the reflection coefficient of the double-ridged horn antenna DRH20 [40], in front of which the tag was placed at a distance of 20 cm. The far field for the diagonal of the horn aperture of 0.1 m in size was around 0.2 m at 3.2 GHz, so the condition for the assessment of RCS was fulfilled. The RCS response of the tag was calculated using relations given in [41] as:

$$\sigma^{tag} = 20\log\left|\frac{S_{11}{}^{tag} - S_{11}{}^{iso}}{S_{11}{}^{ref} - S_{11}{}^{iso}}\right|\sigma^{ref}, \tag{4}$$

where $S_{11}{}^{tag}$ is the reflection coefficient when the measured tag was used as a scatterer. In turn, $S_{11}{}^{ref}$ symbolizes the reflection coefficient when a reference metallic plate was used as a scatterer. Next, $S_{11}{}^{iso}$ represents the reflection coefficient of the antenna itself when no scatterer was installed and comprises residual reflection from the experiment environment. Finally, σ^{tag} is the RCS of the measured tag while σ^{ref} is the RCS of the reference scatterer, which was a rectangular metal plate with dimensions of a × b = 45 × 30 mm^2 (similar to those of the measured tag) and a thickness of 0.3 mm. The analytical formula for the reference scatterer RCS was given in [42] as:

$$\sigma^{ref} = 4\pi\frac{a^2b^2}{\lambda^2}, \tag{5}$$

where λ is the signal wavelength in free space.

The monostatic measurement arrangement made it possible to avoid angle-dependent formulas for reference scatterers and to eliminate the influence of the mutual coupling between the transmitting and receiving antennas in the bistatic measurement. A frequency sweep of the vector network analyzer was performed over a frequency range of 1.5 GHz (2.5 to 4 GHz) in order to detect the RCS resonant peaks that served to distinguish tag peaks.

However, resonant peaks represented the frequency shift in the RCS response of the tag, which depended on the energy input given by the generator consequently from the voltage across the varactor diode while supposing that the transmission loop of the WPT was placed at a distance of 10 mm.

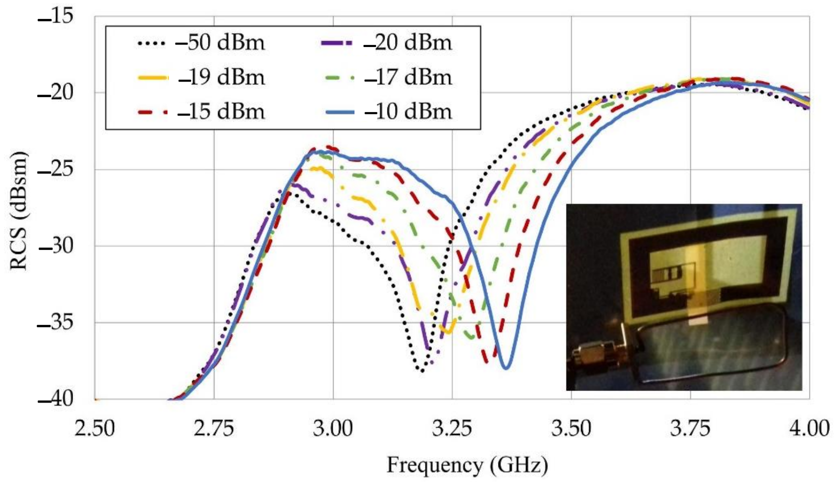

Figure 12. Measured RCS for different values of input power P_g.

It is important to underline that the measurement results given in Figure 12 show a good agreement with the simulation data presented in Figure 3. A direct comparison in a common figure was not appropriate because the model (Figure 3) did not include the exact physical geometry of the WPT power loop location, but the capacitance of the discrete capacitor was set here directly using the discrete element parameters in the simulator. In contrast, in the measurement case, the actual geometry was considered, including the change in varactor capacitance via the voltage induced across the power loop and rectified. Taking these differences into account, the shape similarity of the waveforms in Figures 3 and 12 together with the corresponding resonant dip shift was considered a good agreement between the simulations and measurements.

The curve $P_g = -10$ dBm represented the highest resonance frequency. This corresponded to the maximum voltage at which we had a minimum capacitance. Figure 3 also shows that for the lowest capacitance, we obtained the maximum resonance frequency. As a result, the same continuous tuning range of 200 MHz from 3.2 to 3.4 GHz was achieved.

Changing the varactor capacitance depending on DC bias would slightly change the Q-factor of the resonator, which may have affected the detection tolerance. This change was very small in a given voltage range, as can be seen in Figure 12. The repeatability of the sensor was also an important issue. Verification of these effects was not the focus of this manuscript; we only aimed to present a proof of concept. This issue will need to be thoroughly verified before any real deployment of such a sensor. However, considering the relatively small frequency variations, the need for individual calibration can be assumed.

Table 6 compares the properties of the concept presented here with relevant published acetone sensors operating in the microwave frequency band [22–25]. Although the relative sensitivity of the presented solution was lower than some results published by other authors, these structures were mostly detected by direct measurements over a cable or, in a few cases, wirelessly over a short distance. In fact, the remote sensing structure proposed in our paper showed a better RCS response that outperformed the referenced competitors. This, together with the possibility of baseband detuning, can be considered as the main contribution of this paper. Future research will address the issue of further improving the performance of the sensitive phthalocyanine layer. The presented solution was similar in principle to the previously published solution [14]; however, the benefit of the approach presented here lies in the ability to realign the fundamental resonant frequency using WPT. The advantage of our solution compared to that in [23] is the possibility of the independent design of the WPT and the reading part. The WPT loop must be placed relatively close to the tag due to sufficient efficiency; however, the actual reading of the RCS response (and hence the information) can be performed at a substantially larger distance. This can be achieved by using the structure with increased RCS response.

Table 6. Comparison of properties of microwave acetone sensors.

#	Type of Sensor Structure	f_0 (GHz)	Δf (kHz/ppm)	RCS (dBsm)	Notch (dB)	Contactless
1	[22] Microstrip line	8.5	15,200	-	-	no
2	[23] Ring resonators	4	40	−30	14	15 mm
3	[24] Split-ring reson.	5.5	30	−25	10	no
4	[25] Open gap reson.	7.4	17	-	-	no
5	[14] ID U-dip in loop	3.4	1.2	−18	16	500 mm
6	This work	3.2–3.4 sweep	1.2	−20	18	500 mm

4. Conclusions

In this paper, a proof of concept of the idea of the fusion of a sensor tag with a frequency tuning using WPT was presented. A reconfigurable chipless tag powered with WPT and used as a gas sensor was successfully designed and fabricated. This tag was applied to the sensor, which consisted of a rectangular loop coupled to a U-folded resonator loaded with a glide-symmetrical interdigital capacitor with a thin film of tetrasulfonated copper phthalocyanine applied as a sensitive layer. New experimental verification confirmed the sensor's capability to detect chemical vapors (see Table 2). Furthermore, a varactor diode was used to ensure the reconfigurability of the sensor. The varactor diode was biased with a WPT system operating at a frequency of 7.2 MHz. Changing the DC voltage controlled the resonant frequency of the RCS response. A continuous tuning range of 200 MHz was achieved and confirmed experimentally. This tuning helped to set up the maximal sensitivity of the sensor for a particular type of vapor. A possible higher-frequency detuning can be achieved by using a parallel connection of several varactors.

The proposed external control of the resonant frequency of various resonant circuits can be applied to a wide range of electric resonators that will be used in various sensing applications in the forthcoming IoT era.

Author Contributions: Conceptualization, H.A., J.M. and M.S.; Methodology, H.A., N.B., J.M. and M.S.; Software, H.A. and M.S.; Validation, H.A., J.M. and M.S.; Writing—original draft preparation, H.A.; Writing—review and editing, J.M., M.S. and N.B.; Visualization, J.M., M.S. and N.B.; Supervision, J.M. and L.L.; Funding acquisition, J.M. and M.S. All authors have read and agreed to the published version of the manuscript.

Funding: This work was funded by the Ministry of Education, Youth and Sports of the Czech Republic (program: INTER-EXCELLENCE; subprogram: INTER-COST; project: LTC20012) and the COST – European Cooperation in Science and Technology (COST Action CA18223 SyMat).

Institutional Review Board Statement: Not applicable.

Informed Consent Statement: Not applicable.

Data Availability Statement: Data sharing not applicable.

Acknowledgments: Not applicable.

Conflicts of Interest: The authors declare no conflict of interest.

References

1. Want, R. An introduction to RFID technology. *IEEE Pervasive Comput.* **2006**, *5*, 25–33. [CrossRef]
2. Tharindu, A.; Karmakar, N. Chipped versus chipless RF identification: A comprehensive review. *IEEE Microw. Mag.* **2019**, *20*, 47–57.
3. Li, H.N.; Ren, L.; Jia, Z.G.; Yi, T.H.; Li, D.S. State-of-the-art in structural health monitoring of large and complex civil infrastructures. *J. Civ. Struct. Health Monit.* **2016**, *6*, 3–16. [CrossRef]
4. Herrojo, C.; Mata-Contreras, J.; Paredes, F.; Martín, F. Microwave encoders for chipless RFID and angular velocity sensors based on S-shaped split ring resonators. *IEEE Sens. J.* **2017**, *17*, 4805–4813. [CrossRef]
5. Cui, L.; Zhang, Z.; Gao, N.; Meng, Z.; Li, Z. Radio frequency identification and sensing techniques and their applications—A review of the state-of-the-art. *MDPI Sens.* **2019**, *19*, 4012. [CrossRef]

6. Dey, S.; Saha, J.K.; Karmakar, N.C. Smart sensing: Chipless RFID solutions for the internet of everything. *IEEE Microw. Mag.* **2015**, *16*, 26–39. [CrossRef]
7. Kaneko, M.; Hu, W.; Hayashi, K.; Sakai, H. Compressed sensing-based tag identification protocol for a passive RFID system. *IEEE Commun. Lett.* **2014**, *18*, 2023–2026. [CrossRef]
8. Kracek, J.; Mazanek, M. Wireless power transmission for power supply: State of art. *Radioengineering* **2011**, *20*, 457–463.
9. Team, C.A.I. Europe and the Future for WPT: European Contributions to Wireless Power Transfer Technology. *IEEE Microw. Mag.* **2017**, *18*, 56–87. [CrossRef]
10. Kracek, J.; Svanda, M. Analysis of Capacitive Wireless Power Transfer. *IEEE Access* **2019**, *7*, 26678–26683. [CrossRef]
11. Kracek, J.; Svanda, M.; Hoffmann, K. Scalar Method for Reading of Chipless RFID Tags Based on Limited Ground Plane Backed Dipole Resonator Array. *IEEE Trans. Microw. Theory Tech.* **2019**, *67*, 4547–4558. [CrossRef]
12. Li, C.; Tan, Q.; Zhang, W.; Xue, C.; Xiong, J. An embedded passive resonant sensor using frequency diversity technology for high-temperature wireless measurement. *IEEE Sens. J.* **2014**, *15*, 1055–1060.
13. Salmerón, J.F.; Albrecht, A.; Kaffah, S.; Becherer, M.; Lugli, P.; Rivadeneyra, A. Wireless chipless system for humidity sensing. *Sensors* **2018**, *18*, 2275. [CrossRef] [PubMed]
14. Svanda, M.; Machac, J.; Polivka, M.; Havlova, S.; Fitl, P.; Vrnata, M. Chipless RFID Tag with Enhanced RCS Used as a Phthalocyanine-Based Solvent Vapors Sensor. *IEEE Antennas Wirel. Propag. Lett.* **2020**, *19*, 1556–1560. [CrossRef]
15. Occhiuzzi, C.; Rida, A.; Marrocco, G.; Tentzeris, M. RFID passive gas sensor integrating carbon nanotubes. *IEEE Trans. Microw. Theory Tech.* **2011**, *59*, 2674–2684. [CrossRef]
16. Hallil, H.; Chebila, F.; Menini, P.; Aubert, H. Feasibility of passive Gas sensor based on whispering gallery modes and its RADAR interrogation: Theoretical and experimental investigations. *Sens. Transducers J.* **2010**, *116*, 38–48.
17. Occhiuzzi, C.; Cippitelli, S.; Marrocco, G. Modeling, design and experimentation of wearable RFID sensor tag. *IEEE Trans. Antennas Propag.* **2010**, *58*, 2490–2498. [CrossRef]
18. Naqui, J.; Martín, F. Microwave sensors based on symmetry properties of resonator-loaded transmission lines. *J. Sens.* **2015**, *2015*, 741853. [CrossRef]
19. Zhang, P. Design and Fabrication of Chemiresistor Typemicro/Nano Hydrogen Gas Sensors Using Interdigitated Electrodes. Ph.D. Thesis, University of Central Florida, Orlando, FL, USA, 2008.
20. Ali, M.A.; Chen, M.M.C.; Chen, J.C.M.; Wu, C.T.M. Microwave gas sensor based on graphene-loaded substrate integrated waveguide cavity resonator. In Proceedings of the 2016 IEEE MTT-S International Microwave Symposium (IMS), San Francisco, CA, USA, 22–27 May 2016.
21. Ebrahimi, A.; Beziuk, G.; Scott, J.; Ghorbani, K. Microwave differential frequency splitting sensor using magnetic-LC resonators. *Sensors* **2020**, *20*, 1066. [CrossRef]
22. Rydosz, A.; Maciak, E.; Wincza, K.; Gruszczynski, S. Microwave-based sensors with phthalocyanine films for acetone, ethanol and methanol detection. *Sens. Actuators B Chem.* **2016**, *237*, 879–886. [CrossRef]
23. Abbasi, Z.; Zarifi, M.H.; Shariati, P.; Hashisho, Z.; Daneshmand, M. Flexible Coupled Microwave Ring Resonators for Contactless Microbead Assisted Volatile Organic Compound Detection. In Proceedings of the 2017 IEEE MTT-S International Microwave Symposium (IMS), Honolulu, HI, USA, 4–9 June 2017; pp. 1228–1231.
24. Zarifi, M.H.; Sohrabi, A.; Shaibani, P.M.; Daneshmand, M.; Thundat, T. Detection of Volatile Organic Compounds Using Microwave Sensors. *IEEE Sens. J.* **2015**, *15*, 89–99. [CrossRef]
25. Wiwatcharagoses, N.; Parkm, K.Y.; Chahal, P. Metamaterial-Inspired Sensor on Porous Substrate for Detection of Volatile Organic Compounds in Air. In Proceedings of the Electronic Components and Technology Conference, Las Vegas, NV, USA, 31 May–3 June 2016; pp. 1557–1562.
26. Yang, F.; Qiao, Q.; Virtanen, J.; Elsherbeni, A.Z.; Ukkonen, L.; Sydanheimo, L. Reconfigurable sensing antenna: A slotted patch design with temperature sensation. *IEEE Antennas Wirel. Propag. Lett.* **2012**, *11*, 632–635. [CrossRef]
27. Jiang, Z.; Yang, F. Reconfigurable sensing antennas integrated with thermal switches for wireless temperature monitoring. *IEEE Antennas Wirel. Propag. Lett.* **2013**, *12*, 914–917. [CrossRef]
28. Tawk, Y.; Christodoulou, C.G. A new reconfigurable antenna design for cognitive radio. *IEEE Antennas Wirel. Propag. Lett.* **2009**, *8*, 1378–1381. [CrossRef]
29. Chaabane, G.; Madrangeas, V.; Chatras, M.; Arnaud, E.; Huitema, L.; Blondy, P. High-Linearity 3-bit frequency-tunable planar inverted-F antenna for RF applications. *IEEE Antennas Wirel. Propag. Lett.* **2017**, *16*, 983–986. [CrossRef]
30. Ayadi, H.; Machac, J.; Beldi, S.; Latrach, L. Planar Hexagonal Antenna with Dual Reconfigurable Notched Bands for Wireless Communication Devices. *Radioengineering* **2021**, *30*, 25–33. [CrossRef]
31. Amin, E.M.; Saha, J.K.; Karmakar, N.C. Smart sensing materials for low-cost chipless RFID sensor. *IEEE Sens. J.* **2014**, *14*, 2198–2207. [CrossRef]
32. Beeresha, R.S.; Khan, A.M.; Manjunath-Reddy, H.V. Design and optimization of interdigital capacitor. *Int. J. Res. Eng. Technol.* **2016**, *5*, 73–78.
33. Skyworks. SMV121x Series: Hyperabrupt Junction Tuning Varactors. Available online: https://datasheet.lcsc.com/szlcsc/Skyworks-Solutions-SMV1213-001LF_C150866.pdf. (accessed on 28 July 2016).
34. Kracek, J.; Svanda, M.; Mazanek, M.; Machac, J. Implantable semi-active UHF RFID tag with inductive wireless power transfer. *IEEE Antennas Wirel. Propag. Lett.* **2016**, *15*, 1657–1660. [CrossRef]

35. Takhedmit, H.; Cirio, L.; Picon, O.; Vollaire, C.; Allard, B.; Costa, F. Design and characterization of an efficient dual patch rectenna for microwave energy recycling in the ISM band. *Prog. Electromagn. Res. C* **2013**, *43*, 93–108. [CrossRef]
36. Chandravanshi, S.; Akhtar, M.J. An efficient dual-band rectenna using symmetrical rectifying circuit and slotted monopole antenna array. *Int. J. RF Microw. Comput. -Aided Eng.* **2020**, *30*, e22117. [CrossRef]
37. INFINEON. BAS3007A: Low VF Schottky Diode Array. Available online: https://www.infineon.com/dgdl/Infineon-BAS3007ASERIES-DS-v01_01en.pdf?fileId=db3a3043156fd5730115a286aa19083b (accessed on 20 November 2007).
38. Tomecek, D.; Hruska, M.; Fitl, P.; Vlcek, J.; Maresova, E.; Havlova, S.; Patrone, L.; Vrnata, M. Phthalocyanine photo-regeneration for low power consumption chemiresistors. *ACS Sens.* **2018**, *3*, 2558–2565. [CrossRef] [PubMed]
39. Diodes 1SMB5920B—1SMB5956B: 3.0W surface mount power zener diode. Available online: https://www.diodes.com/assets/Datasheets/ds32125.pdf (accessed on 1 May 2020).
40. RF Spin, DRH20: Double Ridged Waveguide Horn. Available online: https://www.rfspin.cz/en/antennas/measurement-antennas/drh20 (accessed on 2 June 2021).
41. Polivka, M.; Havlicek, J.; Svanda, M.; Machac, J. Improvement in robustness and recognizability of RCS response of U-shaped strip-based chipless RFID tags. *IEEE Antennas Wirel. Propag. Lett.* **2016**, *15*, 2000–2003. [CrossRef]
42. Added, M.; Boulejfen, N.; Svanda, M.; Ghannouchi, F.M.; Vuong, T.P. High-performance chipless radio-frequency identification tags: Using a slow-wave approach for miniaturized structure. *IEEE Antennas Propag. Mag.* **2019**, *61*, 46–54. [CrossRef]